Impact of Diurnal Warm Layers on Atmospheric Convection

Radomyra Shevchenko[1], Cathy Hohenegger[1], and Mira Schmitt[2]

[1]Max Planck Institute for Meteorology, Hamburg, Germany
[2]Leibniz Institute for Baltic Sea Research, Warnemünde, Germany

Key Points:

- Diurnal warm layers increase atmospheric moisture.
- The increase of cloud cover following the formation of a diurnal warm layer is immediate and only lasts for several hours.
- The magnitude of the cloud cover increase is small and has no discernible influence on the global mean.

Corresponding author: Radomyra Shevchenko, radomyra.shevchenko@mpimet.mpg.de

Abstract

This manuscript presents a study of oceanic diurnal warm layers in kilometer-scale global coupled simulations and their impact on atmospheric convection in the tropics. With the implementation of thin vertical levels in the ocean, diurnal warm layers are directly resolved, and sea surface temperature (SST) fluctuations of up to several Kelvin appear in regions with low wind and high solar radiation. The increase of SST during the day causes an abrupt afternoon increase of atmospheric moisture due to enhanced latent heat flux, followed by an increase in cloud cover and cloud liquid water. However, although the daily SST amplitude is exaggerated in comparison to reanalysis, this effect only lasts for 5-6 hours and leads to an absolute difference of 1% for cloud cover and 0.01 kg m^{-2} for cloud liquid water. All in all, the impact of diurnal warm layers on convective cloud cover is found to be negligible in the tropical mean.

Plain Language Summary

The daily fluctuations of sea surface temperature (SST) have been extensively studied for the last decades, but the assessment of importance of this phenomenon for atmospheric convection on the global scale has come within reach only very recently, thanks to the development of simulations with a horizontal resolution of O(1 km). In this manuscript we show that we can indeed observe an impact of SST fluctuations on moisture in the atmosphere. However, the impact on the amount of cloud in the tropics is found to be short-lived and its magnitude negligible on average.

1 Introduction

Diurnal sea surface temperature anomalies and their interplay with the atmosphere and in particular with the diurnal cycle of convection have been an object of study for many decades. In this study, we investigate this connection for the first time using simulations that can explicitly resolve both the daily temperature variations in the ocean and convection in the atmosphere on a global scale.

Daily variations in sea surface temperature (SST) have already been described in Sverdrup et al. (1942). Since then, there have been numerous studies describing the physics and the conditions of appearance of daily sea surface temperature (SST) variations, the seminal work by Price et al. (1986) being the first detailed description of this phenomenon. Under low-wind conditions and with sufficient insolation, a stable near-surface layer forms during the day in the upper layers of the ocean (until the depth of O(10 m)) that leads to a surface warming of up to 5 K (see Wick and Castro (2020)). In absence of solar radiation during the night, the stratification dissolves as vertical turbulent mixing takes overhand, until a homogeneous mixed layer is restored. The physics of this phenomenon is described in detail in a monograph by Soloviev and Lukas (2013). This stratified, warm layer is known as diurnal warm layer (DWL) and it is ubiquitous in all latitudes, causing SST fluctuations of 0.2 K or more in the entire Northern hemisphere and beyond during boreal summer (see Gentemann et al. (2003)). A comprehensive discussion of its definition and properties can be found in a review by Kawai and Wada (2007). In particular, the authors of the review point out that the presence of DWLs in observations as well as in single column simulations leads to stronger latent and sensible heat fluxes. As surface fluxes connect the surface to the atmospheric boundary layer and since changes in boundary layer properties affect the development of convection, the question of the impacts of DWLs on atmospheric convection arises.

Investigating this question in models requires both fine enough vertical resolution in the ocean, to resolve DWLs, and fine enough horizontal grid spacing in the atmosphere, to resolve atmospheric convection. With the development of deca- to kilometer scale simulations in a coupled configuration such investigations are becoming possible. Prominent

among the newest studies are the papers by Voldoire et al. (2022) and Brilouet et al. (2021). In Voldoire et al. (2022), a single column coupled model has been considered, while in Brilouet et al. (2021), a one column ocean model has been coupled to an atmospheric large-eddy simulation model integrated over a limited area. Both experiments are based on or validated with the data from the Dynamics of the Madden Julian Oscillation (DYNAMO) campaign, during which daily SST differences of several Kelvin were observed. Voldoire et al. (2022) showed that the impact of DWLs on the boundary layer depth, atmospheric moisture and precipitation seems to be small. In contrast, de Szoeke et al. (2021) argued that in the observations from the DYNAMO data set, convection is enhanced on days with large SST differences. Finally, Voldoire et al. (2022) conjectured that a single column model cannot capture horizontal interactions that might lead to a larger impact.

To the authors' knowledge, there is yet no study extending the question of interactions between DWLs and atmospheric convection to a realistic, global framework with resolved convection. And yet, atmospheric convection plays a key role in the energy and water cycle in the tropics, therefore describing the driving mechanisms of convection and assessing their importance is crucial.

The present study aims at closing this gap and precisely analysing the impact of DWLs on atmospheric convection in a global, coupled ICON simulation with 5km horizontal resolution and decameter grid spacing in the first oceanic layers. This allows us to resolve DWL and convection, to assess their interactions, also by resolving horizontal gradients, and to analyse the global impacts of DWLs. We are particularly interested in understanding whether the presence of DWLs enhances cloud cover in a time frame of several days and if so, whether this happens through a direct moistening by the latent heat flux or by enhancing spatial gradient in SST and mesoscale circulations. Moreover, the global nature of our simulation allows to zoom in on different areas and encompass other meteorological and sea conditions than the ones of the DYNAMO campaign.

The manuscript is structured as follows. In Section 2 we describe the setup of the experiments, and in Section 3 we analyse the representation and properties of DWLs in global ICON simulations. In Section 4 we quantify the effect of DWLs on surface fluxes, atmospheric moisture and clouds, and finally in Section 5 we present the conclusions of our work.

2 Experimental setup

To study the effect of DWLs, we conduct global coupled simulations with the ICON model in its Sapphire configuration. The Sapphire configuration targets simulations with a horizontal grid spacing finer than 10 km. For our simulations, we use a setup similar to the simulation called `G_AO_5km` in Hohenegger et al. (2022), with small deviations that will be described below. The model is fully coupled, and at the horizontal resolution of approximately 5 km it is at the boundary of resolving convection. Although the cloud amount associated with shallow convection is expected to be overestimated (see Vial et al. (2019) and Hohenegger et al. (2020)), it has been demonstrated in Vial et al. (2019) that both amplitude and shape of the daily cloud cycle remain similar for horizontal resolutions varying between 150 m and 2.5 km in ICON simulations. This setup allows us to directly access how an SST anomaly influences convection, to study possible interactions between clouds and DWLs in a highly realistic context, and to analyse global implications of including DWLs into models.

The main prerequisite for resolving DWLs in ocean simulations is high vertical resolution of the upper oceanic layers (cf. Brilouet et al. (2021)). The introduction of the z^* ocean coordinate into the ICON model (detailed in Singh and Korn (in preparation)) allows running global experiments with an unprecedented vertical resolution. For the pur-

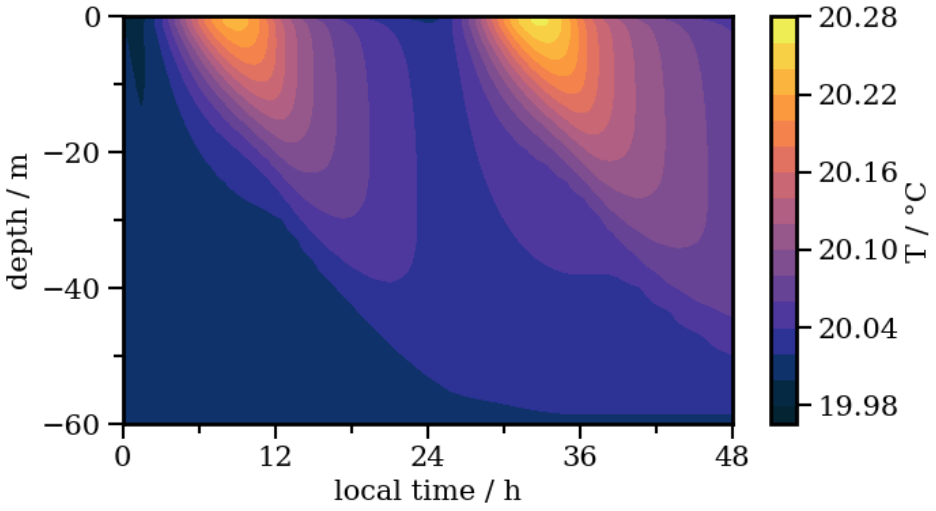

Figure 1: 48h simulation of DWLs in GOTM with the resolution specified in Figure A1 for an idealised heatflux with a maximal radiation of 600 W m^{-2}, a constant wind speed of 8 m s^{-1}, and a time step of 80 s.

poses of this article, we conducted two simulations. One has 128 ocean vertical levels, starting at 2 m at the surface and gradually growing with depth, which is also the setup in `G_AO_5km` in Hohenegger et al. (2022). This simulation plays the role of the reference simulation. The other has 139 ocean vertical levels, starting with 0.5 m and gradually increasing and blending into the reference setup from 45.4 m depth (see Figure A1 in the Appendix). To determine layer thicknesses necessary for resolving DWLs, while keeping the total number of layers as low as possible, we ran test simulations with the one dimensional ocean model GOTM (Umlauf et al. (2005)). The vertical grid that we chose is sufficiently coarse to obtain a numerically stable global run and produces DWLs whose temperature field is indistinguishable in its depth, magnitude and overall vertical structure from a run with a 10 cm uniform grid (see Figure A2 in the Appendix and Figure 1). We run both simulations for 30 days starting January 21 2020 and with the coupling and radiation time steps of 12 min, the atmosphere time step of 30 s, and the ocean time step of 80 s. Both simulations have identical initial conditions, whereby the generation of the initial ocean state is described in Hohenegger et al. (2022). We call the runs with 128 and 139 ocean levels S_{control} and $S_{+\text{DWL}}$ respectively.

3 Representation of diurnal warm layers

In this section we describe the features of DWLs as represented in our simulations and compare them to known properties derived from measurements, reanalysis, and limited-area decameter-scale simulations. As our main focus is on tropical convection, we concentrate our analysis on the tropics which we define here as the area comprised between 40°N and 40°S.

3.1 Occurrence and magnitude

First we diagnose DWLs and assess their occurrence and magnitude. Rigorously speaking, DWLs are defined via vertical temperature gradients (see e.g. Matthews et al. (2014)), as they represent a temperature anomaly sitting on top of the ocean mixed layer. Instead of the temperature gradient, the daily SST amplitude (DSA) is often used as a

proxy (e.g. in Voldoire et al. (2022)), because, as mentioned in Bellenger and Duvel (2009), in the tropics one can assume that horizontal advection happens at longer time scales, and the temperature changes in the upper ocean can be attributed to DWLs. We also adopt this approach, formally defining DWLs as places with DSA larger than 0.1 K, which corresponds to non-zero depth of a DWL in Matthews et al. (2014). Care is required when following this approach, as SST in our model is defined as the temperature in the uppermost layer. In $S_{+\mathrm{DWL}}$ it is the average temperature over 0.5 m and in S_{control} the average temperature over 2 m. Since in this study our main interest is the response of the atmosphere, and since this is the temperature that the atmosphere sees, we do not correct for this difference in our analysis.

In our simulations, DWLs are ubiquitous: Even spots with DSA of over 1.5 K cover 5% of the tropical ocean area. Comparing DWLs in our simulations and in ERA5 reanalysis, we can see in Figure 2 that for the last 10 days of January the spatial distribution of DWLs is in good agreement with each other, with a correlation coefficient of 0.51. The major hot spots of DWLs are in the Indian ocean south of the equator, along the western coasts of America and Africa, and in the southern part of the Pacific, both in our simulations and in ERA5. Similar areas are also identified in the January climatology map of Bellenger and Duvel (2009). A striking feature of our simulation is that, while for S_{control} the DSA field appears nearly homogeneous and the extremes are underestimated compared to ERA5, as expected from the use of thick ocean vertical layers, the amplitudes in $S_{+\mathrm{DWL}}$ are much larger than in the reanalysis, with values twice as high. This is in contrast with observations summarised in Kawai and Wada (2007). Since Kawai and Wada (2007) employed the skin temperature to diagnose DWL, we can conclude that DSA is overestimated in $S_{+\mathrm{DWL}}$. This is confirmed by further observations. The PIRATA buoys located at 0°N10°W and 0°N0°E at 1 m depth have each measured DSA of under 0.7 K in the same period, and the average DSA measured during the EUREC^{4}A field campaign in the area 56.5°W−59°W and 12°N−14.5°N is about 0.15 K, while in $S_{+\mathrm{DWL}}$ the values at these locations are 1.8 K and 0.71 K respectively. A possible cause for the overestimation is insufficient vertical mixing in the upper layers of the ocean. As this study concentrates on the atmospheric effect of the DWLs, this problem does not jeopardise the analysis, and if anything indicates that the simulated effects will be too strong.

Another important feature is that in $S_{+\mathrm{DWL}}$, DWLs tend to avoid areas with high cloud cover: on a given day, 24% of cells over the ocean have a cloud cover of 0.9 or higher, while for cells where DWLs develop this number reduces to 13%. However, there are also many areas with a low cloud cover and yet no significant DWLs, as shown in Figure 3. For instance, out of all areas with cloud cover below 0.3 on a given day, only 9% developed DWLs with DSA of 1.5 K or higher. This is a consequence of a property well documented in observational studies. Indeed, as explained in Soloviev and Lukas (2013), shortwave radiation and surface wind are the two principal driving factors of DWLs, where high shortwave radiation and low wind speed favor the appearance of DWLs. The previously mentioned areas with low cloud cover but no DWL correspond to high-wind zones. The relationship of DWLs with downward shortwave radiation and near-surface wind speed will be further explored in Section 3.2.

As to the horizontal extent of DWLs as simulated by $S_{+\mathrm{DWL}}$, there are two observations to be made. As shown in Figure 4a, there are many small clusters of DWLs, but the total area they cover is practically negligible: although 177 clusters out of 799 are of size ≤ 625 km^2, the total area covered by them amounts to only 0.3% of the entire area covered by DWLs. On the opposite end of the histogram in Figure 4a, one can see that there are a few clusters of size 10^6 km^2. They form predominantly in the high DSA areas from Figure 2 (not shown). Moreover, for each particular grid cell, the DWLs do not seem to be persistent: for instance, in a region with very high DSA in the Indian ocean (between 70°E−75°E and 5°S−10°S, see the white square in Figure 2b) during a period of 30 days no episode of DSA$>$ 0.6 K lasted longer than ten days, and 80% of all episodes

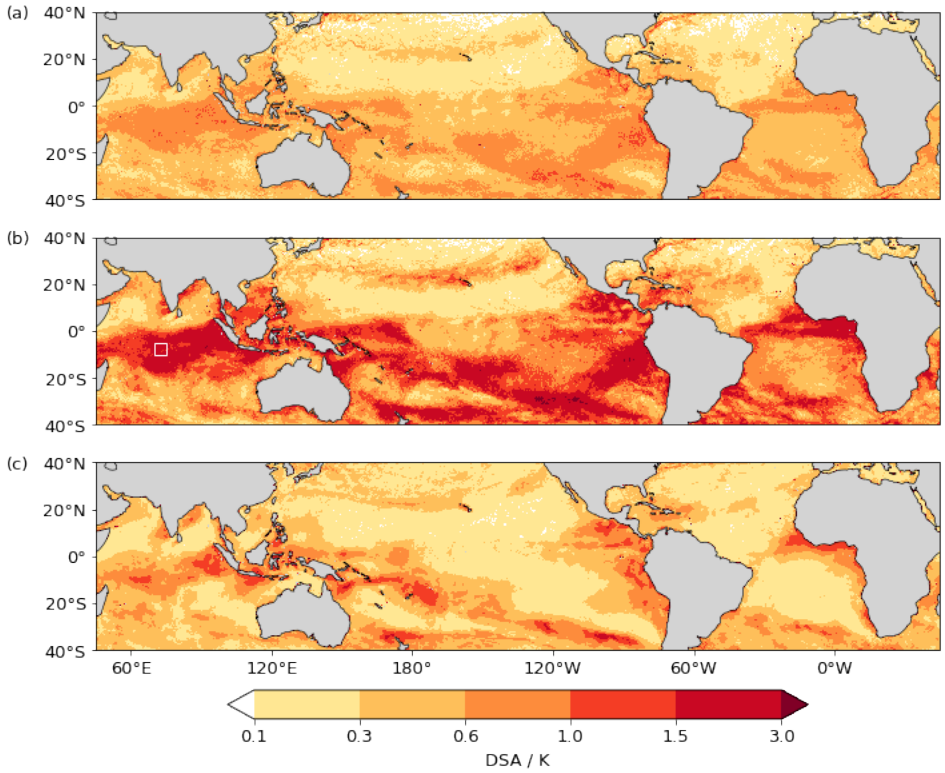

Figure 2: Magnitudes of the daily SST amplitude (max−min), averaged between 22 and 30 January 2020 in (a) $S_{control}$, (b) S_{+DWL}, and (c) ERA5. The white rectangle in (b) designates an area in the Indian ocean that is analysed in Section 3.1.

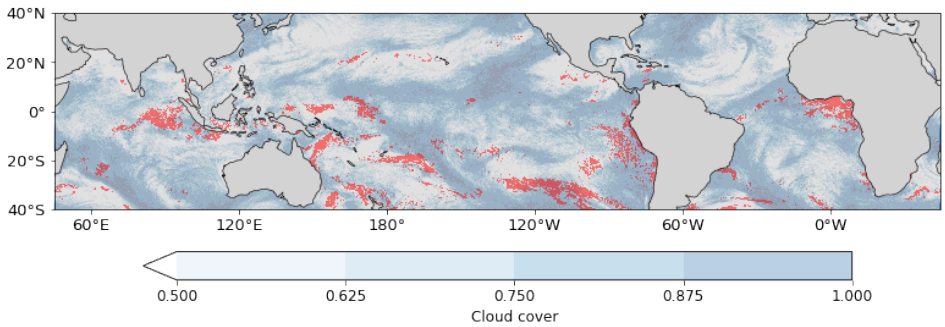

Figure 3: Cloud cover on a particular day (23 January 2020) in S_{+DWL}. Red areas correspond to DWL regions with DSA of over 1.5 K.

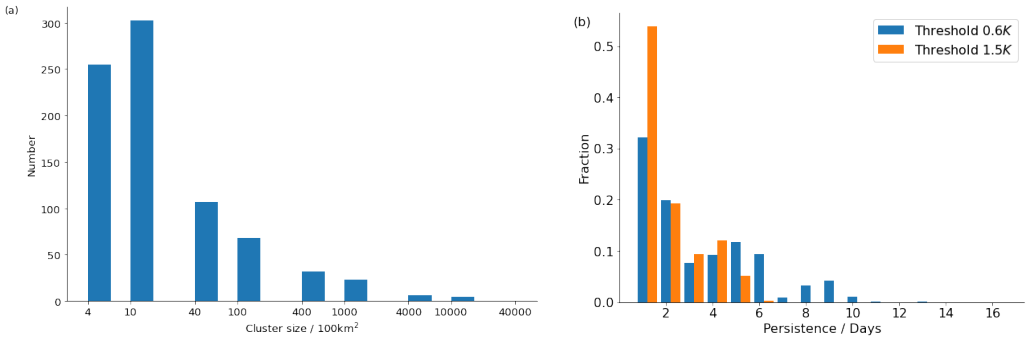

Figure 4: (a) Clusters of DWLs to the threshold of 1.5 K on a particular day (23 January 2020) ordered in a histogram of cluster sizes. (b) Normalised histogram of DWL episode lengths to different thresholds for the box 70°E−75° E and 5°S−10°S

.

lasted five days or less (see Figure 4b). Expectedly, the persistence time becomes shorter if a higher threshold for DSA is considered. This result is similar to the findings in the ERA40 forced simulation in Bellenger and Duvel (2009), where they showed that the DWL episode duration decays faster than exponentially.

3.2 Structure of DWLs and preconditions for their formation

For a deeper understanding of how the known properties of DWLs are captured by S_{+DWL} we focus on a study of this phenomenon in the tropical northern Atlantic region off the coast of Barbados, more precisely in the box 56.5°W−59°W and 12°N−14.5°N corresponding to the region of the EUREC^{4}A field campaign (Stevens et al. (2021)).

First, we examine the vertical structure of a DWL produced in the simulation S_{+DWL}. As shown in the anomaly profile (Figure 5), the incoming heat quickly accumulates in the upper layers during the day, as the warming of the upper layers creates a stable stratification if the mixing is slow, which is the case under low wind conditions. During the night, the DWL slowly dissipates until a single mixed layer is restored. As mentioned before, in this region, the heat anomalies are overestimated: a typical DSA in glider observations is approximately 0.15 K (see Hohenegger et al. (2022), Figure 11c), while in S_{+DWL} in a calm period it is around 0.3 K. The time of the maximum and minimum is captured accurately compared to these observations (about 16 h LT and 8 h LT respectively).

Another analysis demonstrates that the dependency of DSA on insolation and surface wind observed, among others, in satellite measurements in Gentemann et al. (2003), are reproduced in ICON simulations as expected, namely higher DSA correlates with lower winds and higher downward shortwave radiation at the surface. The scatterplot in Figure 6a shows a relationship similar to the formula

$$\text{DSA} \sim \begin{cases} U^{-3} \text{ for } U < \text{4-5 m s}^{-1}, \\ U^{-1} \text{ for } U > \text{4-5 m s}^{-1}, \end{cases}$$

suggested in Soloviev and Lukas (2013) for 10 m wind speed U, although the threshold appears to be located at 6−7 m s^{-1} rather than at 4-5 m s^{-1}. Also the linear dependence on shortwave radiation described in Matthews et al. (2014) seems to be confirmed in S_{+DWL} (Figure 6b). In particular, the slope of the linear regression between DSA and surface downward shortwave radiation in ICON is 0.0023 K W^{-1}m^2, which is indeed close

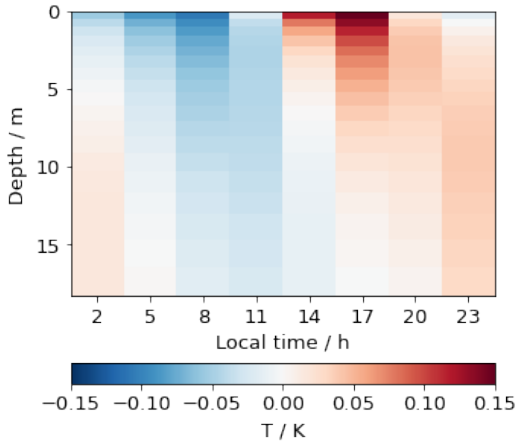

Figure 5: Sea water temperature (3 h output) averaged over 3 days over the box 56.5°W-59°W and 12°N-14.5°N, time anomaly.

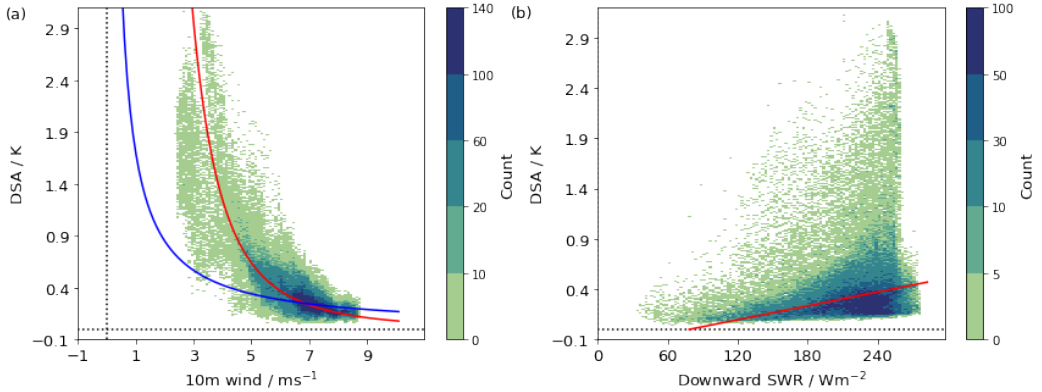

Figure 6: 2D histograms of SST amplitude and (a) 10 m wind speed as well as (b) shortwave radiation over the box 56.5°W to 59°W and 12°N to 14.5°N in S_{+DWL}. The blue and red lines in (a) indicate the interpolation of U^{-1} and U^{-3} to higher and lower wind speeds respectively. The red line in (b) is the linear regression fit between the variables.

to the slope of 0.0021 K W^{-1}m^2 found in Matthews et al. (2014). The large scattering of points in Figure 6b is caused by the joint influence of wind speed and radiation on DWLs.

4 Effect of DWLs on convection

The previous section shows that DWLs are frequent in the tropics, they cover large areas and persist over several days. We can therefore hypothesize that they might have an effect on atmospheric convection, either by creating horizontal air temperature gradients, or by enhancing the moistening of the overlying air. Moreover, as DSA in S_{+DWL} is overestimated, the effect of DWLs is expected to be too strong.

To assess the impact of DWLs on convective clouds, we need to compare the values of relevant variables in places where DWLs develop to places where they do not develop. A clean way to accomplish this without having to account for other sources of variability is to compare the differences between these values in S_{+DWL} and $S_{control}$ at places

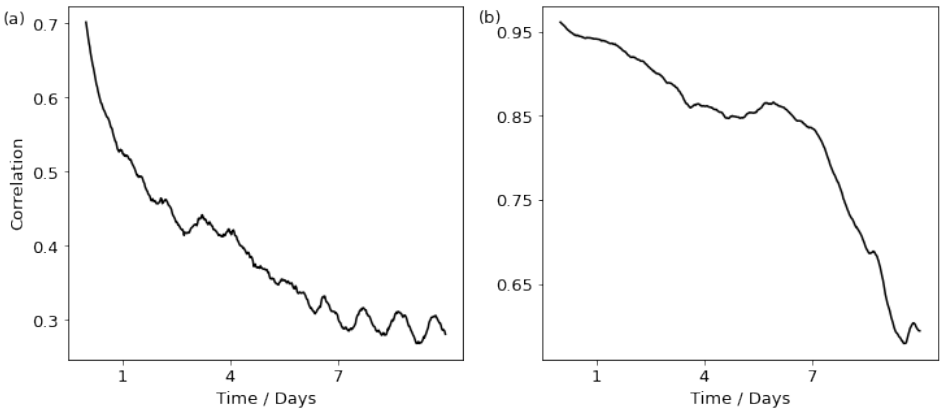

Figure 7: Temporal evolution of the global correlation between $S_{control}$ and S_{+DWL} for (a) cloud cover and (b) latent heat flux.

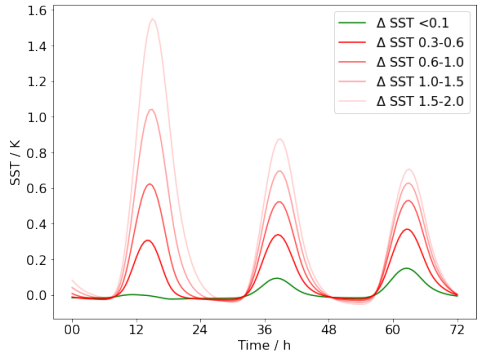

Figure 8: Time series (in local time) of S_{+DWL}-$S_{control}$ for different ΔSST.

where DWLs of a certain magnitude are present in S_{+DWL}. A key point in this analysis is to only include the first 4 days after the start of the simulation into the investigation to ensure that the two simulations remain close and do not diverge due to the chaotic nature of the atmosphere. Figure 7 shows that both simulations indeed remain highly correlated during the first several days.

To conduct our analysis, we proceed as follows. The ocean is subdivided into 0.25°× 0.25° disjoint squares, and for each square the hourly maximal SST difference between S_{+DWL} and $S_{control}$ during a day, denoted by ΔSST, is computed. Based on this first day of the analysis that we also call the detection day, two groups can be formed: one called the "no DWL difference" group, where ΔSST stays below 0.1 K, and another one where ΔSST lies between certain thresholds T_1 and T_2, which we call the "DWL difference between T_1 and T_2" group. Note that the plot of ΔSST yields a map very similar to Figure 2b (Figure B1 in the Appendix), and thus can be used as a proxy for identifying DWL areas. We use this proxy from now on to cover a larger variety of cases and to obtain a cleaner comparison.

The subsequent analysis consists in comparing the two groups to each other, focusing on the time series of the differences in relevant variables over the days 1-3, with day 1 being the detection day, see Figure 8 for an example of the differences in SST. Statistically, it is supported by t-tests for equality of means for independent samples with

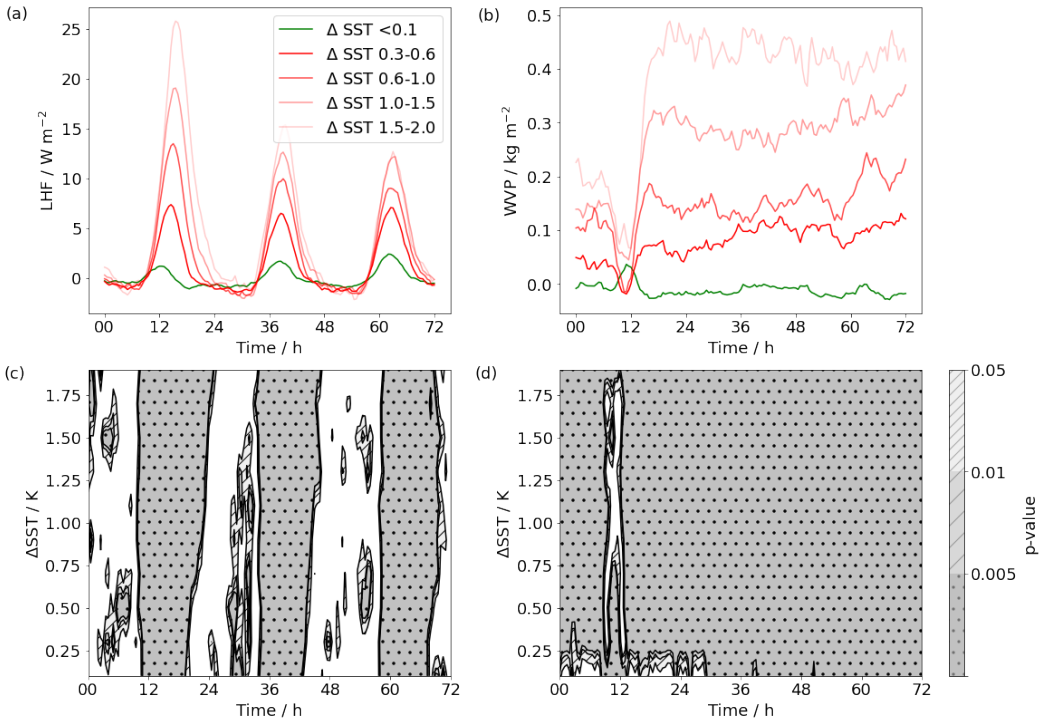

Figure 9: Time series (in local time) of S_{+DWL}-$S_{control}$ and t-test significance levels in bins of 0.1 K for LHF (a, c) and WVP (b, d). On panel c and d, white means not significant.

different variances. Every group with $T_2 - T_1 = 0.1$ K has at least 1695 cells, a sufficient number to ensure the robustness of the results. The size of the squares is chosen in accordance to the cluster sizes discussed in Section 3.1 (see Figure 4), as a mesoscale analysis is sufficient to capture a possible effect of DWLs, and also because the temperature and moisture changes produced by one isolated cell of $0.1° \times 0.1°$ are not expected to have a large effect and would be quickly mixed in the atmosphere. Moreover, we make the assumption that the effects in cloudiness are localised. Indeed, the impact of DWLs on cloud cover via moistening is a local effect, and the mesoscale circulation created by SST gradients would also result in cloud formation over DWLs. With this assumption, the samples can be treated as independent.

4.1 Impact on latent heat flux and related quantities

First we investigate whether higher ΔSST leads to more moisture in the air over DWL areas. This will help understand whether cloud formation may be impacted over DWLs. In particular, we are going to concentrate on differences in latent heat flux (LHF) and water vapor path (WVP) to measure the effects on evaporation and column moistening respectively, as shown in Figure 9.

The first observation concerning the plots (a, b) in Figure 9 is that the differences between S_{+DWL} and $S_{control}$ in the "no DWL difference" group after the detection day revolve around zero, as expected and further justifying our approach. This is not the case for the "DWL" groups. Differences are clearly appearing and are of larger magnitude, the stronger the DWL is.

The latent heat flux is increased when DWLs are present, with a peak around noon on every day, as expected from the daily cycle in SST. WVP is always higher over DWLs. The difference decreases in the morning hours of the detection day and increases rapidly thereafter. The dip could be caused either by a dip in LHF, by an increase of precipitation or by a weakening in convergence of moisture. As LHF is increased and there is no excessive rain over DWLs (not shown), the dip must be due to weaker convergence, which might be caused by a weakening of surface wind required for DWL formation. The increase of WVP after 12 h LT reflects the increase in moisture due to increased LHF. One can trace the propagation of the moisture response to DWLs in Figure 9, since the onset and duration times of the effects are different: while LHF reacts immediately and is tied directly to differences in temperature (see Figure 8), the effect on WVP is delayed by several hours and persists over the following days without losing its magnitude.

Figure 9(c, d) confirms that the differences observed visually are highly significant even on the third day and even for small ΔSST with p-values smaller than 0.005, except for the nighttime values of LHF. However, an important point is that the absolute differences are rather small, especially for smaller ΔSST: For instance, for ΔSST between 0.6 K and 1.0 K, the peak of LHF is below 15 W m^{-2} and WVP is below 0.2 kg m^{-2}. One can compare these values with global averages of the two quantities over the ocean, which are ca. 130 W m^{-2} for LHF and ca. 34.6 kg m^{-2} for WVP. The order of magnitude of LHF changes is similar to that found in the single column configuration in Voldoire et al. (2022).

4.2 Impact on cloudiness

The variables we consider for analysing the impact of DWLs on clouds are cloud cover (CC) and cloud liquid water (CLW).

The responses of CC and CLW shown in Figure 10 are very similar to each other. The "no DWL difference" time series is fluctuating around zero after the detection day, but on the detection day itself there is a peak at midday. In contrast, the DWLs regions exhibit dips at the same time, and the magnitude of these dips is positively correlated with the ΔSST amplitude (see Figure 10(a, b) and Figure 10(e, f)). This illustrates the prerequisite for DWLs to exist mentioned in Section 3.1: The appearance of DWLs is generally favored by a lower cloud amount. Subsequently we can observe the cloud response to the formation of DWLs on the detection day: after about 12 h LT, the difference between S_{+DWL} and $S_{control}$ in both CC and CLW over DWLs starts to grow, and by 15 h LT both simulations have the same cloud amount. This growth is statistically significant starting from an SST amplitude of 0.3 K, and the effect persists longer for higher values of ΔSST, namely until 20 h LT for ΔSST of 1.5-2.0 K and until 18 h LT for ΔSST of 0.3-1.0 K for CC. Moreover, the effect seems to last longer for CLW, although the values of both variables fall back below the zero line already during the night. In total, the increase of cloud following the formation of a DWL lasts up to 5-6 h.

A behaviour similar to the first day, that is, less CC and CLW in S_{+DWL} compared to $S_{control}$ in the morning and rise of these quantities in S_{+DWL} in the afternoon, can be observed also on the second and third day after the detection day (Figure 10(a, b)), however, the deviation is barely significant: most of the time, the p-value is above 0.05, especially for higher values of ΔSST (Figure 10(c, d)). This means that the increase of the quantities is often not homogeneous enough to be interpreted as systematic (see Figure 10(c, d)). A crucial factor here is the absolute magnitude of the differences: In extreme cases, for ΔSST between 1.5 and 2.0 K, the deviation of CC reaches 0.03 and that of CLW 0.02 kg m^{-2} on the detection day. On the following day the corresponding maximal values fall to 0.01 and 0.01 kg m^{-2}, while the averages are 0.001 and 0.002 kg m^{-2} respectively (see Figure 10(a, b)). We can compare those to the average values of CC and CLW over DWLs, 0.65 for CC and 0.11 kg m^{-2} for CLW. The average increase in CLW is about

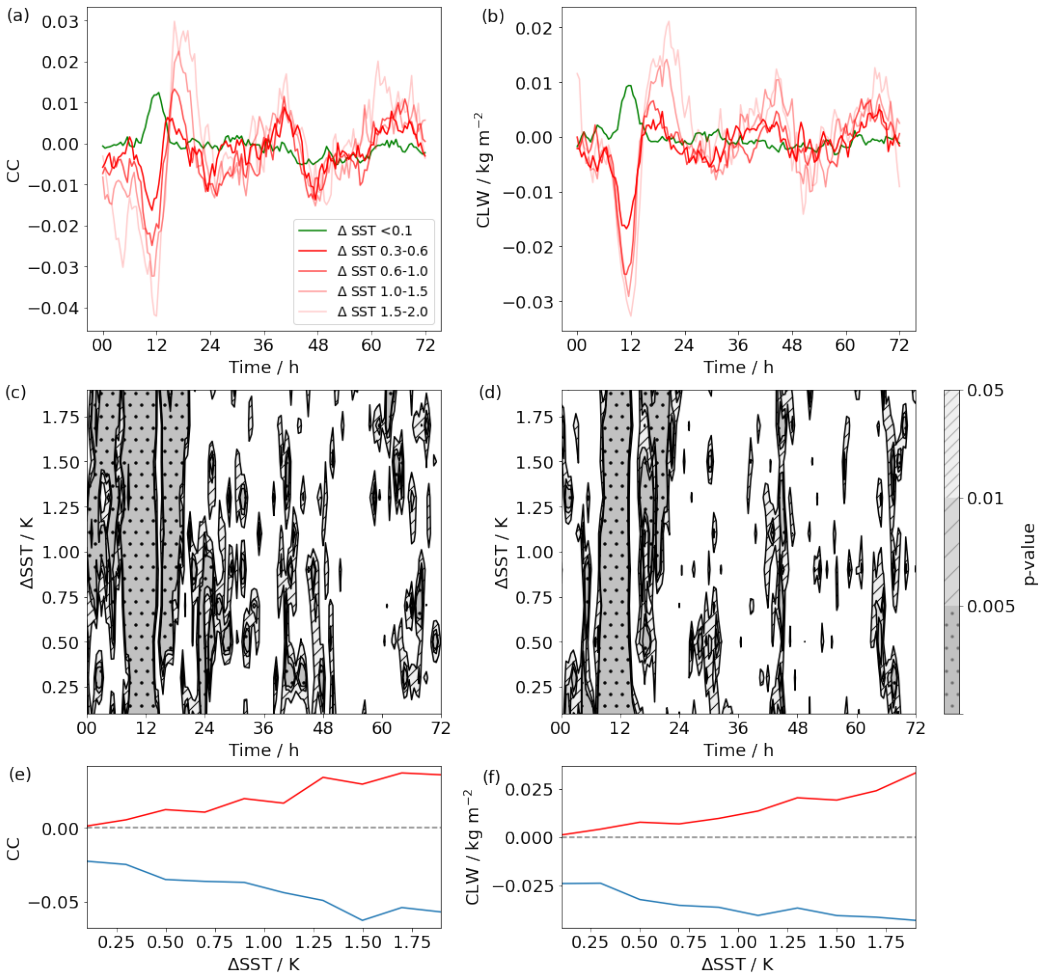

Figure 10: Time series (in local time) of S_{+DWL}-$S_{control}$, t-test significance levels in bins of 0.1 K, and maximal (red) and minimal (blue) value of the deviation on the detection day for CC (a, c, e) and CLW (b, d, f).

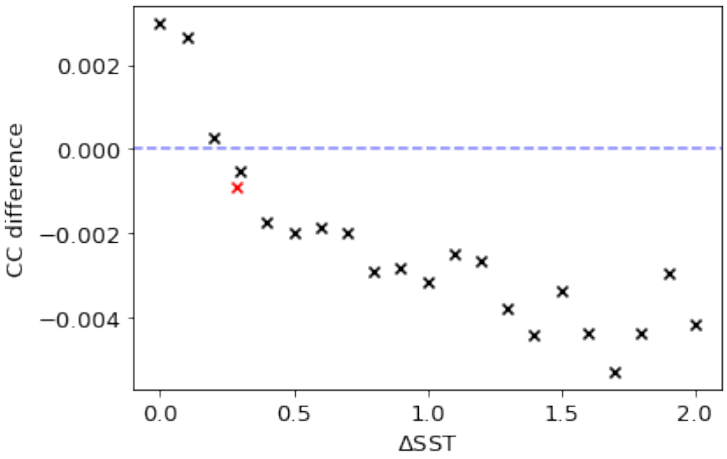

Figure 11: Daily mean CC differences (S_{+DWL}-$S_{control}$) as a function of ΔSST (black crosses). The red cross is the average CC difference against the average ΔSST.

1% and the increase in CC is about 0.2% on the day following even very large ΔSST. We can therefore conclude that the effect on the cloud water content is higher than the contribution of DWLs to cloud cover change, but the effects are very small.

The morning/midday dip of CC and CLW over DWLs even overcompensates the subsequent rise of these quantities. Figure 11 shows mean CC differences between S_{+DWL} and $S_{control}$ as a function of ΔSST on the detection day. For ΔSST above 0.3 K the simulation S_{+DWL} has lower values of CC than $S_{control}$, and only for ΔSST below 0.3 K the reverse is true, such that on average, S_{+DWL} has slightly less cloud than $S_{control}$. The effect of DWLs appears to be dominated by the variability of the model. All in all, we can conclude that DWLs do not increase the global mean of cloud cover or cloud liquid water path.

We continue the analysis by looking at deep and shallower clouds separately, as one might expect to see more effects associated with one type of clouds. We differentiate between deep and shallow clouds by taking the outgoing longwave radiation at the top of the atmosphere of 240 W m^{-2} as a threshold. This value is mentioned in Fu et al. (1990) as the threshold often used to identify deep convection. While the figures for shallower clouds are very similar to Figure 10 (not shown), the deviation for CLW in deep clouds is somewhat larger, up to 0.03 kg m^{-2} on the detection day. As shown in Figure 12a for CC, the effects, despite being a bit larger, remain very small and do not exhibit systematic significance (Figure 12c). Considering precipitation as an additional possibility to see an impact of DWLs (Figure 12(b, d)), we see that there is no sufficient evidence to attribute the fluctuations of precipitation, even for higher values of ΔSST, to anything more than chance.

The last question that we want to investigate is to what extent the presence of DWLs might affect the diurnal cycle of convection. We focus on the example of the EUREC^{4}A field campaign, which took place in the northern tropical Atlantic. For this region the diurnal cycle of shallow convection has been studied in great detail in Vial et al. (2019). In particular, it has been shown there that, in observations as well as in large-eddy simulations (LES), the cloud cover peaks during the day, which might make it more susceptible to SST in comparison to other regions. In our case, both S_{+DWL} and $S_{control}$ over-

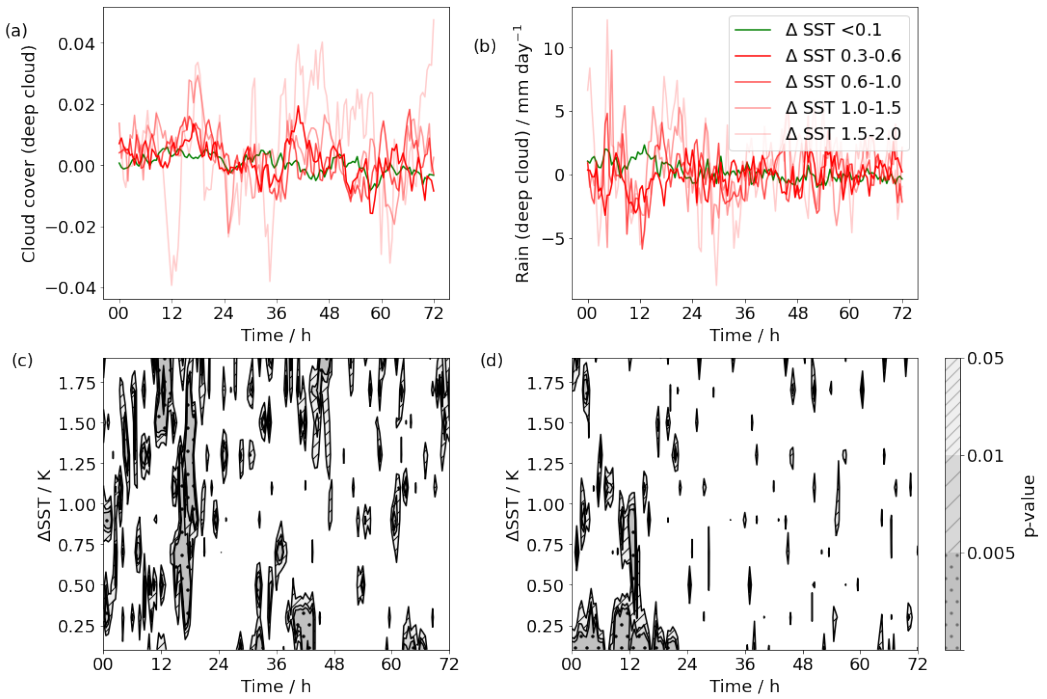

Figure 12: As Figure 9, but for CC (a, c) and precipitation (b, d) associated with deep convection.

estimate the CC found in observations by a factor of 2, as was expected from the resolution sensitivity study in Vial et al. (2019), but capture perfectly the time structure as well as the amplitude of the cycle: minimum between 12 and 15 LT, maximum at 2 LT, amplitude of about 0.1 (Figure 13), in good agreement with observations in Vial et al. (2019). The increase in CC resulting from the appearance of DWLs occurs in the late-afternoon. If anything, CC slightly decreases at other times. Both effects taken together tend to slightly reduce the diurnal amplitude. The fact that DWLs only have a small influence on the diurnal cycle of CC is consistent with the study in Vial et al. (2019) that reproduced the main features of the cycle in LES despite using fixed SST.

5 Discussion and conclusions

By introducing thin vertical levels into the global coupled ICON model, we could directly resolve diurnal warm layers (DWLs) and assess their impact on the atmosphere. The simulations employed a grid spacing of 5 km, both in the atmosphere and ocean, so that ocean mesoscale eddies and atmospheric convection can be resolved explicitly. The DWLs produced by the simulation reproduce the physical features known from observations and limited area decameter simulations, but the magnitude of the daily SST fluctuations is exaggerated in comparison to reanalysis, by about a factor of two.

The increase in the amplitude of the diurnal cycle of SST in regions with diurnal warm layers leads to a corresponding increase in latent heat flux (LHF) and water vapor path (WVP). The effects are significant, even on days 2 and 3 following the detection of a diurnal warm layer, but the values are small: 7 W m^{-2} difference in LHF and 0.1 kg m^{-2} difference in WVP for a SST difference of 0.6 K. In the late-afternoon of the detection day, cloud cover (CC) and cloud liquid water (CLW) content also increase, but the effects are small and lose statistical significance within 5-6 hours of appearance. What

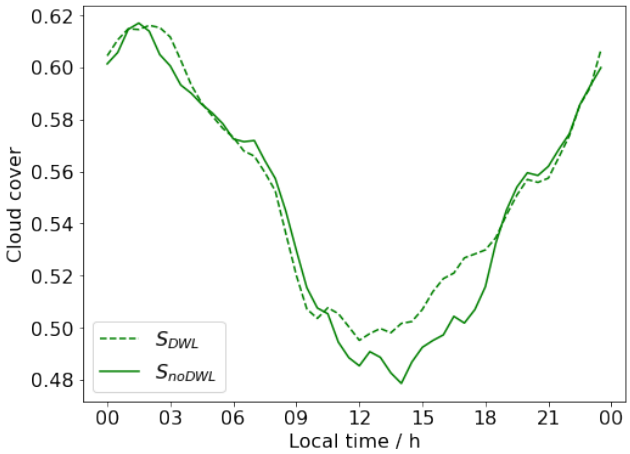

Figure 13: Diurnal cloud cover cycle in the box 56.5°W to 59°W and 12°N to 14.5°N, composite over 30 days.

is however significant is a decrease in cloud cover and liquid water content on the day of detection, around noon. This expresses the fact that diurnal warm layers favorably form in areas of low cloud cover, and hence high insolation. This effect compensates the subsequent increase. All in all, resolving diurnal warm layers does not affect the mean cloud cover over tropical oceans.

The amplitude of the observed differences in LHF is simuliar to findings in Voldoire et al. (2022), and the impact on cloud cover shows that convection over DWLs is enhanced, as it is claimed in the observation study of de Szoeke et al. (2021). Moreover, the small influence of DWLs on the CC cycle in the tropical Atlantic supports the results in Vial et al. (2019). A surprising and unprecedented finding of our study is the impact of DWLs on convection remains small even for a strongly enhanced daily SST amplitude over this particular region as well as globally.

We finish the discussion by focusing on the implications and limitations of our study. Regarding the question of the importance of DWLs in models, one needs to differentiate between the local and the overall impact. In our exemplary study in the northern tropical Atlantic, the presence of DWLs can reduce the amplitude of the diurnal cycle of the cloud cover by up to 10% (see Figure 13). In some specific cases with extraordinarily high DSA, DWLs might indeed play a role. However, this remains a rare phenomenon.

The analysis in this manuscript only concerns short-term effects of DWLs. However, it is known that the mean SST increases in DWL areas (Bellenger and Duvel (2009)). Therefore, inclusion of DWLs will have a long-term influence on the energy budget that is not treated here, but at least for short-term effects, our study demonstrates that DWLs do not have a global and significant impact.

Appendix A Vertical resolution of the simulations

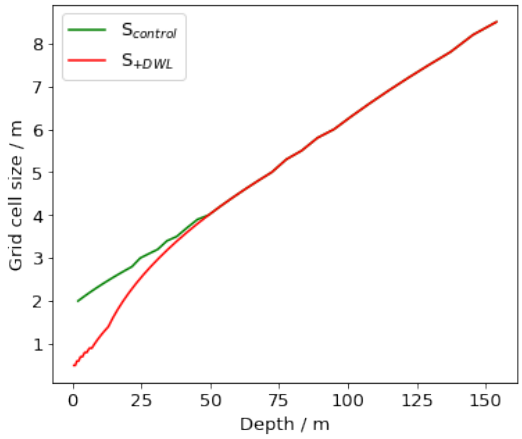

Figure A1: Layer thicknesses for S_{+DWL} and $S_{control}$

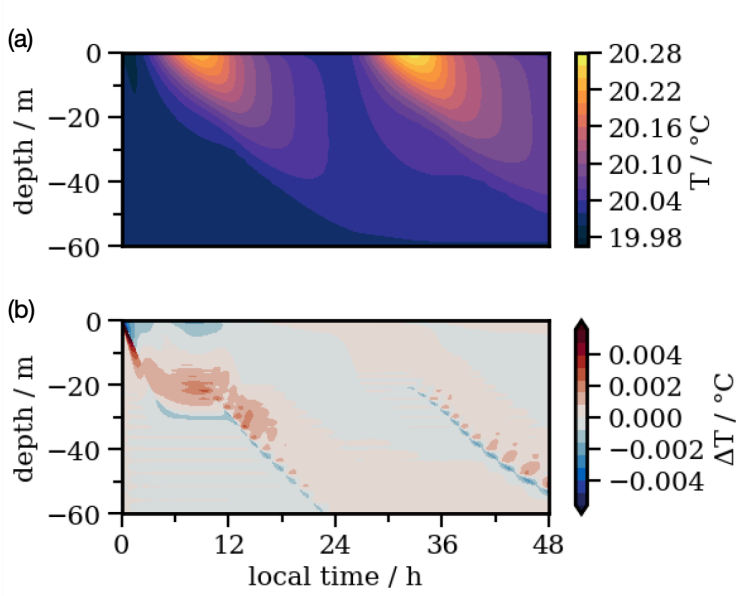

Figure A2: (a) As in Figure 1, but with uniform 0.1 m thick vertical layers. (b) Difference between the temperature profiles in Figure 1 and (a).

Appendix B Average ΔSST as proxy for DSA

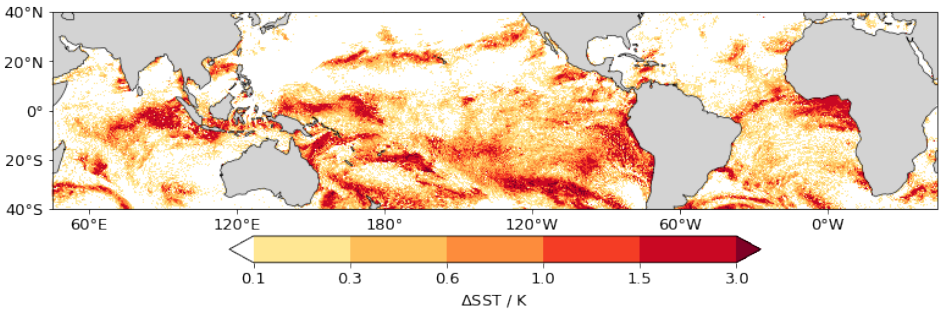

Figure B1: ΔSST on detection day.

Appendix C Open Research

Detailed information concerning the ICON model is contained in the publication Hohenegger et al. (2022). The ocean model GOTM is documented in Umlauf et al. (2005) and can be installed from `https://gotm.net`. The ERA5 dataset used in this study has been provided by the Climate Data Store.

Acknowledgments

This work used resources of the Deutsches Klimarechenzentrum (DKRZ) granted by its Scientific Steering Committee (WLA) under project ID bm1253. The authors gratefully acknowledge the support of the DFG-funded collaborative research centre TRR181 "Energy Transfers in Atmosphere and Ocean".

References

Bellenger, H., & Duvel, J.-P. (2009). An analysis of tropical ocean diurnal warm layers. *Journal of Climate*, *22*(13), 3629 - 3646. Retrieved from `https://journals.ametsoc.org/view/journals/clim/22/13/2008jcli2598.1.xml` doi: 10.1175/2008JCLI2598.1

Brilouet, P.-E., Redelsperger, J.-L., Bouin, M.-N., Couvreux, F., & Lebeaupin Brossier, C. (2021). A case-study of the coupled ocean–atmosphere response to an oceanic diurnal warm layer. *Quarterly Journal of the Royal Meteorological Society*, *147*(736), 2008-2032. Retrieved from `https://rmets.onlinelibrary.wiley.com/doi/abs/10.1002/qj.4007` doi: https://doi.org/10.1002/qj.4007

de Szoeke, S. P., Marke, T., & Brewer, W. A. (2021). Diurnal ocean surface warming drives convective turbulence and clouds in the atmosphere. *Geophysical Research Letters*, *48*(4), e2020GL091299. Retrieved from `https://agupubs.onlinelibrary.wiley.com/doi/abs/10.1029/2020GL091299` (e2020GL091299 2020GL091299) doi: https://doi.org/10.1029/2020GL091299

Fu, R., Genio, A. D. D., & Rossow, W. B. (1990). Behavior of deep convective clouds in the tropical pacific deduced from isccp radiances. *Journal of Climate*, *3*(10), 1129 - 1152.

Gentemann, C. L., Donlon, C. J., Stuart-Menteth, A., & Wentz, F. J. (2003). Diurnal signals in satellite sea surface temperature measurements. *Geophysical Research Letters*, *30*(3). Retrieved from `https://agupubs.onlinelibrary.wiley.com/doi/abs/10.1029/2002GL016291` doi: https://doi.org/10.1029/2002GL016291

Hohenegger, C., Korn, P., Linardakis, L., Redler, R., Schnur, R., Adamidis, P.,

... Stevens, B. (2022). Icon-sapphire: simulating the components of the earth system and their interactions at kilometer and subkilometer scales. *Geoscientific Model Development Discussions*, *2022*, 1–42. Retrieved from https://gmd.copernicus.org/preprints/gmd-2022-171/ doi: 10.5194/gmd-2022-171

Hohenegger, C., Kornblueh, L., Klocke, D., Becker, T., Cioni, G., Engels, J. F., ... Stevens, B. (2020). Climate statistics in global simulations of the atmosphere, from 80 to 2.5 km grid spacing. *Journal of the Meteorological Society of Japan. Ser. II*, *98*(1), 73-91. doi: 10.2151/jmsj.2020-005

Kawai, Y., & Wada, A. (2007). Diurnal sea surface temperature variation and its impact on the atmosphere and ocean: A review. *Journal of Oceanography*, *63*(5), 721–744. Retrieved from https://doi.org/10.1007/s10872-007-0063-0 doi: 10.1007/s10872-007-0063-0

Matthews, A. J., Baranowski, D. B., Heywood, K. J., Flatau, P. J., & Schmidtko, S. (2014). The surface diurnal warm layer in the indian ocean during cindy/dynamo. *Journal of Climate*, *27*(24), 9101 - 9122. Retrieved from https://journals.ametsoc.org/view/journals/clim/27/24/jcli-d-14-00222.1.xml doi: 10.1175/JCLI-D-14-00222.1

Price, J. F., Weller, R. A., & Pinkel, R. (1986). Diurnal cycling: Observations and models of the upper ocean response to diurnal heating, cooling, and wind mixing. *Journal of Geophysical Research: Oceans*, *91*(C7), 8411-8427. Retrieved from https://agupubs.onlinelibrary.wiley.com/doi/abs/10.1029/JC091iC07p08411 doi: https://doi.org/10.1029/JC091iC07p08411

Soloviev, A., & Lukas, R. (2013). *The near-surface layer of the ocean: Structure, dynamics and applications*. Springer Netherlands. Retrieved from https://books.google.de/books?id=_4zHBAAAQBAJ

Stevens, B., Bony, S., Farrell, D., Ament, F., Blyth, A., Fairall, C., ... Zöger, M. (2021). Eurec^{4}a. *Earth System Science Data*, *13*(8), 4067–4119. Retrieved from https://essd.copernicus.org/articles/13/4067/2021/ doi: 10.5194/essd-13-4067-2021

Sverdrup, H., Johnson, M., & Fleming, R. (1942). *The oceans, their physics, chemistry, and general biology*. Prentice-Hall, Incorporated. Retrieved from https://books.google.de/books?id=h74gAAAAMAAJ

Umlauf, L., Bolding, K., & Burchard, H. (2005). *GOTM – scientific documentation. version 3.2* (Vol. 63). Leibniz-Institute for Baltic Sea Research, Warnemünde, Germany. Retrieved from https://gotm.net/manual/stable/pdf/a4.pdf

Vial, J., Vogel, R., Bony, S., Stevens, B., Winker, D. M., Cai, X., ... Brogniez, H. (2019). A new look at the daily cycle of trade wind cumuli. *Journal of Advances in Modeling Earth Systems*, *11*(10), 3148-3166. Retrieved from https://agupubs.onlinelibrary.wiley.com/doi/abs/10.1029/2019MS001746 doi: https://doi.org/10.1029/2019MS001746

Voldoire, A., Roehrig, R., Giordani, H., Waldman, R., Zhang, Y., Xie, S., & Bouin, M.-N. (2022). Assessment of the sea surface temperature diurnal cycle in cnrm-cm6-1 based on its 1d coupled configuration. *Geoscientific Model Development*, *15*(8), 3347–3370. Retrieved from https://gmd.copernicus.org/articles/15/3347/2022/ doi: 10.5194/gmd-15-3347-2022

Wick, G. A., & Castro, S. L. (2020). Assessment of extreme diurnal warming in operational geosynchronous satellite sea surface temperature products. *Remote Sensing*, *12*(22). Retrieved from https://www.mdpi.com/2072-4292/12/22/3771 doi: 10.3390/rs12223771